Tissue and Cell 78 (2022) 101898

Contents lists available at ScienceDirect

Tissue and Cell

journal homepage: www.elsevier.com/locate/tice

Vitamin D3 supplementation may attenuate morphological and molecular abnormalities of the olfactory bulb in a mouse model of Down syndrome

Fabiana de Campos Gomes [a,b,*], Isabella Boechat Faria Santos [c], Carolinne Makino Stephani [b], Merari de Fátima Ramires Ferrari [d], Orfa Yineth Galvis-Alonso [e], Eny Maria Goloni-Bertollo [a], João Simão de Melo-Neto [c], Érika Cristina Pavarino [a,**]

[a] Genetics and Molecular Biology Research Unit (UPGEM), São José do Rio Preto Medical School (FAMERP), São José do Rio Preto, SP, Brazil
[b] Faculdade de Medicina FACERES, São José do Rio Preto, SP, Brazil
[c] Institute of Health Sciences, Federal University of Pará (UFPA), Belém, PA, Brazil
[d] Department of Genetics and Evolutionary Biology, Biosciences Institute, University of São Paulo (USP), São Paulo, SP, Brazil
[e] Laboratory of Experimental Physiology, São José do Rio Preto Medical School (FAMERP), São José do Rio Preto, SP, Brazil

ARTICLE INFO

Keywords:
Down syndrome
Trisomic mice
Vitamin D_3
Olfactory bulb
Amyloid beta

ABSTRACT

Individuals with Down syndrome (DS) exhibit impaired olfactory function and are at a higher risk of developing Alzheimer's disease (AD). Olfactory dysfunction may be an early clinical symptom of AD. Recent studies have demonstrated that vitamin D3 (VD3) exerts neuroprotective effects in mouse models of AD. In this study, we investigated the effects of VD3 on the morphology, immunolocalization, and markers involved in neuropathogenic processes, apoptosis, proliferation, cell survival, and clearance of amyloid peptides, along with neuronal markers in the olfactory bulb (OB) of an adult female mouse model of DS. Morphological and molecular analyses revealed that trisomic mice exhibited a volume reduction in the external plexiform layer, a decrease in the number of mitral and granule cells, and an increase in the expression of amyloid-β 42, caspase-3 p12, and P-glycoprotein. VD3 reversed certain morphological abnormalities in the OB of control trisomic mice ($Ts_{(CO)}$) and decreased the levels of caspase-3 p12 and methylenetetrahydrofolate reductase in the treated groups. The results demonstrated that trisomy factor causes morphofunctional abnormalities in the OB of $Ts_{(CO)}$ mice. Moreover, VD3 could represent a therapeutic target to attenuate morphological and molecular alterations in OB.

1. Introduction

Down syndrome (DS) is a genetic abnormality caused by trisomy of chromosome 21 (Antonarakis et al., 2004). Trisomy 21 impairs the physiological and morphological development of the brain and leads to the impairment of important functions such as olfactory processing (Murphy and Jinich, 1996; Chen et al. 2006; Cecchini et al., 2016). Olfactory dysfunction in individuals with or without DS has been associated with Alzheimer's disease (AD) (Ter Laak et al., 1994; Cecchini et al., 2016) and may represent an early clinical sign of dementia (Roberts et al., 2016; Zou et al., 2016; Silva et al., 2018).

In DS, olfactory deficits and early onset Alzheimer's disease (EOAD) are observed primarily in adult women and occasionally in men (Hartley et al., 2015; Cecchini et al., 2016; Schupf et al., 2018). Triplication of the beta-amyloid precursor protein (*APP*) located on chromosome 21 is crucial for the development of EOAD in DS (Hartley et al., 2015). The increase in the expression of *APP* and its derivatives contributes to the abnormal production of amyloid-β peptides (Aβ) that primarily include Aβ40 and Aβ42 peptides (Wiseman et al., 2018). Increased production of Aβ42 peptides promotes the deposition and formation of amyloid

Abbreviations: Aβ, amyloid-β; AD, Alzheimer disease; APP, beta-amyloid precursor protein; DS, Down syndrome; EOAD, early-onset Alzheimer's disease; EPL, external plexiform layer; GCL, granule cell layer; GL, Glomerular layer; HE, hematoxylin and eosin; IPL, internal plexiform layer; MCL, mitral cell layer; MTHFR, methylenetetrahydrofolate reductase; NeuN, neuronal nuclei; PBS, phosphate-buffered saline; Pgp, P-glycoprotein; OB, olfactory bulb; VD, Vitamin D; VD3, Vitamin D3.

* Corresponding author at: Genetics and Molecular Biology Research Unit (UPGEM), São José do Rio Preto Medical School (FAMERP), São José do Rio Preto, SP, Brazil.
** Corresponding author.
E-mail addresses: facamposgomes@gmail.com (F.C. Gomes), erika@famerp.br (É.C. Pavarino).

https://doi.org/10.1016/j.tice.2022.101898
Received 28 April 2022; Received in revised form 12 August 2022; Accepted 13 August 2022
Available online 17 August 2022

plaques in different brain regions (Head et al., 2012; Head et al., 2016), including the entorhinal cortex that is involved in olfactory processing (Hof et al., 1995). Decreased neurogenesis in the olfactory bulb (OB) and impaired olfactory function has been reported in Ts65Dn mice (Bianchi et al., 2014); however, the causes of these abnormalities and the relationship between morphological and molecular changes in response to Aβ peptides in the OB remain unknown.

Aβ accumulation may interfere with the processing and transmission of signals across olfactory glomeruli and between cells in different layers of the brain (Ter Laak et al., 1994). Moreover, the increase or deposition of Aβ42 peptides can activate caspase-3-mediated pro-apoptotic mechanisms, trigger inflammation, and consequently lead to neuronal death (Kavanagh et al., 2014; Han et al., 2017).

In contrast, 1,25-dihydroxyvitamin D3 (1,25 [OH]2D3) and Vitamin D3 (VD3) have exhibited neuroprotective effects, including neurogenesis and degradation of Aβ peptides (Anjum et al., 2018). VD3 regulates the expression of mediators involved in Aβ efflux such as P-glycoprotein (Pgp) (Durk et al., 2012; Durk et al., 2014; Landel et al., 2016). Additionally, a possible relationship between VD3 and folate levels has also been previously described (Lucock et al., 2018). Folate metabolism is regulated by methylenetetrahydrofolate reductase (MTHFR). In the folate metabolic pathway, MTHFR is essential for the conversion of folate into metabolites that are used in various cellular processes, including methylation of gene promoters and proteins, amino acids, DNA, and RNA (Spellicy et al., 2012) and in repair processes and cell proliferation (Salbaum and Kappen, 2012; Leclerc et al., 2013).

Additionally, certain studies have suggested an association between *MTHFR* polymorphisms and the risk for AD (Chhillar et al., 2014; Rai, 2017). Alterations in the expression and production of metabolites involved in folic acid metabolism induce DNA demethylation. This may lead to increased expression of certain genes associated with the pathophysiology of AD and those that encode enzymes involved in the cleavage of APP, thus contributing to the increase and deposition of Aβ42 (Román et al., 2019).

Based on these results, we investigated the effects of high doses of VD3 on the morphology, immunolocalization, and expression of the neuronal markers Aβ42, caspase-3 p12, MTHFR, Pgp, and NeuN that are involved in neuropathogenic processes, apoptosis, proliferation, cell survival, and clearance, in the OB of an adult female mouse model of DS.

2. Materials and methods

2.1. Animals

The experimental protocol was performed using six-month-old female mice of lineages B6EiC3Sn-Rb(12. Ts171665Dn)2Cje/CjeDnJ (#004850) and B6EiC3SnF1/J (#001875) that were obtained from the Jackson Laboratory. The mice were maintained at the Institute of Biosciences of the University of São Paulo and the Bioterium of the Medical School of São José do Rio Preto (FAMERP) at a light-dark cycle of 12 h and a temperature of 23 °C (± 2 °C) with appropriate water provided ad libitum and standard chow (Nuvilab®, Curitiba, PR, Brazil).

The experiments were performed in accordance with the regulations of the National Council for the Control of Experiments on Animals (CONCEA). All experimental protocols were approved by the Ethics Committee for Animal Experimentation of FAMERP (Protocol No. 001–002447/2015).

2.2. Experimental groups and treatment

All mice were genotyped at 21 days old to determine the control and trisomic groups (partial trisomy for chromosome 16) according to the protocol described by (Chaves et al., 2020).

Twenty female mice (14 weeks of age) were divided into four experimental groups (five mice per group) that included the $Ts_{(CO)}$ (standard diet with positive genotype), $Wt_{(CO)}$ (standard diet with negative genotype), $Ts_{(VD3)}$ (high-dose VD3 with positive genotype), and $Wt_{(VD3)}$ groups (high-dose VD3 with negative genotype) as presented in Fig. 1.

Mice in the $Wt_{(VD3)}$ and $Ts_{(VD3)}$ groups received a high-dose VD3 diet (12,500 IU/kg; Domeneghetti & Corrêa Ltda®, Jaú, SP, Brazil) for 10 weeks as suggested by Wergeland et al. (2011).

The selection of five animals per experimental group was based on the study by Brianchi et al. (2014). The selection of genotype-positive and genotype-negative animals belonging to the control and experimental groups was randomized. Additionally, to avoid bias in the groups, the trisomic control animals were marked on the ear. In contrast, the trisomic groups were marked with two scratches on the tails in addition to the markings on the ears. This allowed for better control of the animals throughout the experimental period. The next steps of the experimental design were carried out based on the recommendations of the ARRIVE Guidelines (https://arriveguidelines.org/). Only one member of the research team was aware of the allocation of the experimental units to the groups at different time points during the experiment.

2.3. Euthanasia, tissue removal, and processing

At 24 weeks of age, all experimental groups were anesthetized with high-dose (100 mg/kg) intraperitoneal injection of sodium thiopental (Thiopental®). After complete sedation, transcardiac perfusion with phosphate-buffered saline (PBS) was performed, and the brains were removed and dissected to preserve OBs.

The left OB was dissected and fixed by immersion in 4% paraformaldehyde diluted in PBS for 24 h at 4 °C. After fixation, the tissues were embedded in paraffin. The right OB was immersed in liquid nitrogen and stored at − 80 °C for western blotting.

2.4. Stereology and morphology

Coronal sections of the OB (6-μm thick) were created using a microtome. For stereology and morphology, sections were stained with hematoxylin and eosin (HE) and photographed at 400 × magnification using a Zeiss Primo Star microscope coupled to a camera (Zeiss Axiocam 105 color model). Coronal sections of the OB were photographed at intervals of 90 μm thickness (Tsutiya et al., 2016).

For stereology, four systematically randomized sections from each animal (five animals per group) were analyzed using ImageJ software (National Institutes of Health, USA). The stereological method of Weibel et al., (1966) used Weibel's 120-point multipoint grid to measure the relative volumes of the external plexiform layer (EPL), mitral cell layer (MCL), glomerular layer (GL), internal plexiform layer (IPL), and granule cell layer (GCL) (Zhuang et al., 1999). The distances between the point grids were automatically generated and standardized using an

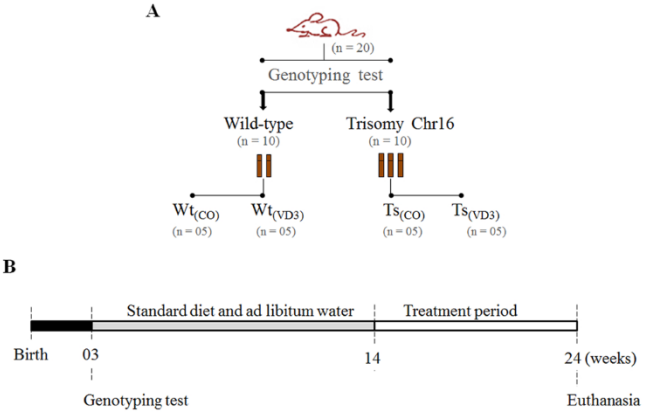

Fig. 1. (A): Experimental groups and (B): timeline of experimental procedures.

analysis program. The mean value of the points within the grid is expressed as a percentage. For morphological analysis, images were acquired at 400x magnification (five systematically randomly selected fields/animal), and 20 histological sections in total were analyzed to count the number of granule and mitral cells (Zhang et al., 2018) using the program ImageJ 1.47 Windows version (National Institute of Health, USA).

2.5. Immunohistochemistry and immunolocalization

The sections were deparaffinized, dehydrated with xylene and ethanol, and subjected to antigen recovery with citrate buffer (pH 6.0). After successive washing steps using PBS, the samples were blocked with endogenous peroxidase containing 3% hydrogen peroxide, and nonspecific proteins were blocked with nonfat milk (MOLICO®) for 1 h at room temperature. Sections were incubated for 2 h at room temperature to detect anti-beta amyloid 1–42 (1:1000 dilution; ab201060). The following day, the sections were washed with PBS and incubated with the secondary antibody (Goat Anti-Rabbit IgG H&L; 1:500, HRP, Abcam ®, USA, ab97051) for 1 h at room temperature. For the negative control, serial sections were incubated with only the secondary antibody. The sections were then washed with PBS, chromogenized with diaminobenzidine (DAB), and counterstained with hematoxylin. The sections were visualized and photographed using a microscope (Camera Zeiss Axiocam 105 color model coupled with a Zeiss Primo Star microscope model at 40 × magnification). The immunolocalization of markers was analyzed using ImageJ 1.47 software Windows version (National Institute of Health, United States Code, USA).

2.6. Western blotting

OB samples from the control and treated groups (five samples per group) were lysed in PBS (pH 7.4) containing 1% Nonidet P-40, 0.5% sodium deoxycholate, 1 mM EDTA, 1 mM EGTA, and 1% SDS that was supplemented with 1% protease inhibitor cocktail (Sigma-Aldrich; St. Louis, MO).

After incubation on ice (30 min), the samples were centrifuged, and the protein fractions were recovered and quantified using the Pierce™ BCA Protein Assay Kit. Three protein pools (each pool corresponding to two different animals) were prepared, being the samples randomly distributed among the three pools, and stored in a freezer at − 80 °C. The pools (25 μg total protein) were then subjected to electrophoresis by 10% or 12% SDS polyacrylamide gels depending upon the molecular weight of each protein.

After electrophoresis, proteins were transferred to a nitrocellulose membrane. The membrane was blocked for 1 h at room temperature with 5% non-fat milk diluted in TBS-T and then incubated overnight at 4 °C with β-actin (1:500; ab8227; abcam®, USA), anti-beta amyloid 1–42 (1:1000; ab201060; abcam®, USA), anti-caspase-3 p12 (1:500; ab179517; abcam®, USA), MTHFR (1:200; ab203789; abcam®, USA), anti-P glycoprotein (1:250; ab170904; abcam®, USA), and anti-NeuN (1:2000; ab177487; Abcam ®, USA) antibodies.

The membrane was washed in TBS-T buffer and incubated with a secondary antibody (Goat Anti-Rabbit IgG H&L; 1:20,000; HRP, Abcam ®, USA, ab97051) for 2 h. The reaction was detected using a chemiluminescent substrate to detect protein bands (Novex™ ECL Chemiluminescent Substrate Reagent Kit).

Semi-quantitative densitometric analyses of the bands were performed using ImageJ 1.47 for Windows (National Institute of Health, United States Code, USA). β-Actin was used as an endogenous control. For quantification of immunoblotting, bands were selected to define the limits of the stops of the detected proteins according to their respective molecular weights. Subsequently, immunoblotting results were analyzed using optical densitometry (quantification of pixels per area). Blots from all sample pools were used to reduce potential errors and variability. β-actin was used as an endogenous control for each protein that was analyzed.

2.7. Statistical analysis

Data were subjected to the Shapiro–Wilk test for normality. Parametric data were analyzed using two-way ANOVA (two factors: treatment and trisomy) with a post-hoc Bonferroni test. The independent variables were trisomy (Ts), vitamin D3 (VD3), and their interactions (Ts and VD3). Effect sizes were assessed as low (0.01–0.33), moderate (0.34–0.66), or high (0.66–0.99) and were analyzed using partial eta squared (ηp2). Nonparametric data were analyzed using the Scheirer–Ray–Hare test and Dunn's test. To determine the sample size and statistical calculation of power, we performed the sample calculation in the program G-power using the following assumptions in ANOVA: fixed effects, omnibus, and one-way. According to the analyses and the work of Hong et al. (2011), the total sample size was eight for the four experimental groups with an actual power of 0.996 ($\beta = 0.8$, $\alpha = 0.05$, effect size $f = 3.28$). Statistical significance was set at $p < 0.05$. The data were analyzed using SPSS software.

3. Results

3.1. Stereology and morphology

The results of stereological and morphological analyses of the experimental groups are presented in Fig. 2. In terms of stereology, Ts mice exhibited a reduction in the volume of the EPL (Fig. 2A). Mice treated with VD3 exhibited an increase in the number of mitral cells (Fig. 2B). There were no significant differences in the IPL or GCL between the experimental groups (Fig. 2C-D).

Morphological analysis revealed that $Ts_{(CO)}$ possessed a lower number of mitral cells ($F = 9.941$, $p = 0.006$; $\eta2 = 0.383$) (Fig. 2E) and granule cells ($F = 6.343$, $p = 0.023$; $\eta2 = 0.284$) (Fig. 2F-G). The number of granule cells in the $Wt_{(VD3)}$ group ($p = 0.049$) (Fig. 2J) was higher than that in the $Wt_{(CO)}$ group.

3.2. Immunostaining and immunoblotting

3.2.1. Trisomic mice exhibited diffuse amyloid deposition and increased expression of Aβ42 and caspase-3 p12 in OB

Aβ42 immunoreactivity was detected in all OB layers of trisomic mice ($Ts_{(CO)}$ and $Ts_{(VD3)}$ groups). In the $Ts_{(CO)}$ group, diffuse plaques of Aβ42 were observed in the EPL and MCL (white arrowhead, Fig. 3A-B). Such plaques were not observed in the EPL of the $Ts_{(VD3)}$ group; however, immunoreactivity was still observed in the layers and was present predominantly in the GL and EPL of the OB (Fig. 3C). In the $Wt_{(CO)}$ group, we detected slight positive immunoreactivity for Aβ42 (Fig. 3D).

The $Ts_{(CO)}$ group exhibited an increased expression of Aβ42 and caspase-3 p12 compared to the $WT_{(CO)}$ group (Fig. 3E-G). After VD3 supplementation, we observed no significant differences in the Aβ42 expression between the $Ts_{(VD3)}$ and $Ts_{(CO)}$ groups (Fig. 3F). However, a reduction in caspase-3 p12 levels was observed in the VD3-treated groups, particularly in $Ts_{(VD3)}$ mice (Fig. 3G).

3.2.2. VD3 reduces MTHFR expression but does not affect Pgp and NeuN expression

The effects of VD3 treatment on the expression of MTHFR, Pgp, and NeuN are indicated in Fig. 4. NeuN expression was not altered in any of the experimental groups (Fig. 4B). VD3 supplementation affected the expression of MTHFR and resulted in decreased levels in the $Ts_{(VD3)}$ and $Wt_{(VD3)}$ groups (Fig. 4C). We determined that trisomic factors contributed to an increase in Pgp in the $Ts_{(CO)}$ group, but Pgp expression in the OB was not altered after VD3 treatment (Fig. 4D).

3.2.3. Possible effects of APP increase in the OB of the $Ts_{(CO)}$ group

To better illustrate the effects of increased expression of APP in the

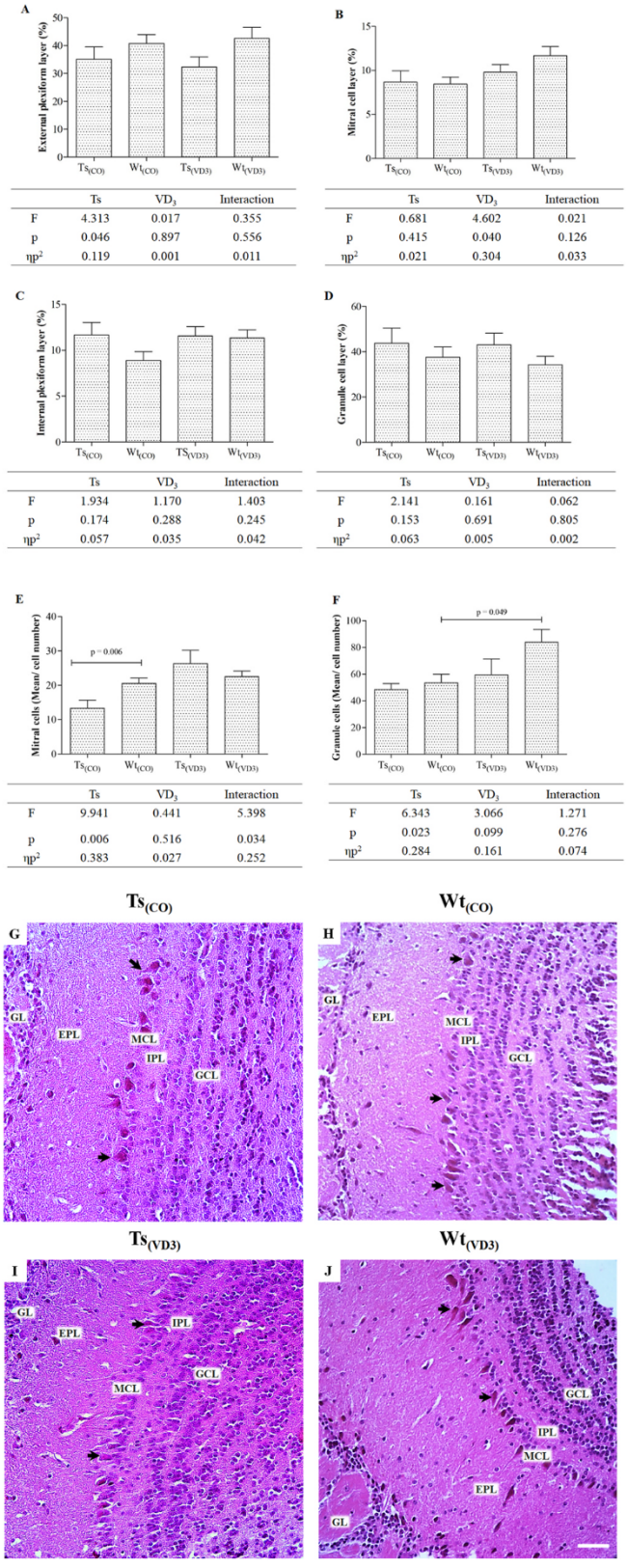

A	Ts	VD_3	Interaction
F	4.313	0.017	0.355
p	0.046	0.897	0.556
ηp^2	0.119	0.001	0.011

B	Ts	VD_3	Interaction
F	0.681	4.602	0.021
p	0.415	0.040	0.126
ηp^2	0.021	0.304	0.033

C	Ts	VD_3	Interaction
F	1.934	1.170	1.403
p	0.174	0.288	0.245
ηp^2	0.057	0.035	0.042

D	Ts	VD_3	Interaction
F	2.141	0.161	0.062
p	0.153	0.691	0.805
ηp^2	0.063	0.005	0.002

E	Ts	VD_3	Interaction
F	9.941	0.441	5.398
p	0.006	0.516	0.034
ηp^2	0.383	0.027	0.252

F	Ts	VD_3	Interaction
F	6.343	3.066	1.271
p	0.023	0.099	0.276
ηp^2	0.284	0.161	0.074

Fig. 2. Stereological analysis and morphology in different layers of the OB in the experimental groups. (A): External plexiform, (B): mitral cell, (C): internal plexiform, and (D): granule cell layer; The rates (in %) of these layers are calculated from the relative volume obtained by multifunctional Weibel grating analysis (A-D); The number of mitral and granular cells is indicated on the histogram (E-F). Images from HE-stained samples revealing the morphological aspects of the olfactory bulb in the (G): $Ts_{(CO)}$, (H): $Wt_{(CO)}$, (I): $Ts_{(VD3)}$, and (J): $Wt_{(VD3)}$ groups. Glomerular layer (GL); external plexiform layer (EPL); mitral cell layer (MCL); internal plexiform layer (IPL); granule cell layer (GCL). Mitral cells (black arrows). Objective magnification: 40x (G-J). Scale bar: 40 μm (G-J).

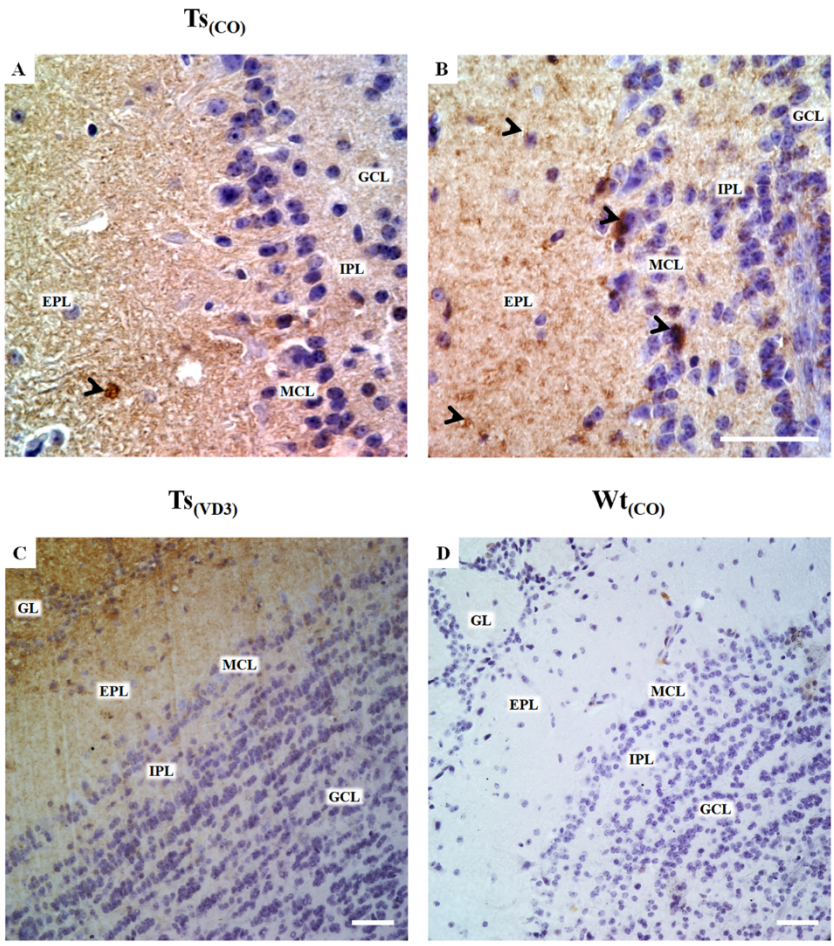

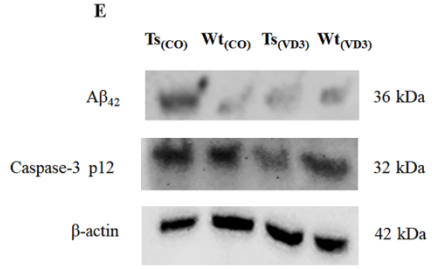

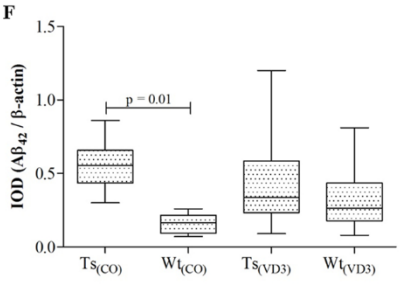

	Ts	VD_3	Interaction
H	8.674	0.041	3.102
p	0.003	0.840	0.078

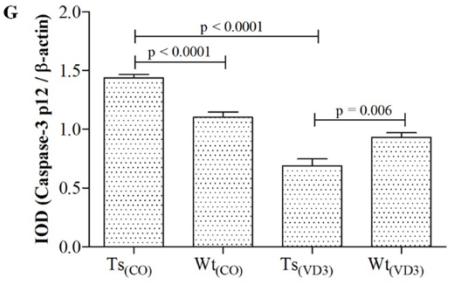

	Ts	VD_3	Interaction
F	1.153	107.729	42.725
p	0.296	<0.0001	<0.0001
ηp^2	0.055	0.843	0.681

Fig. 3. Immunolocalization of $A\beta_{42}$ and immunoblotting for $A\beta_{42}$ and caspase-3 p12. (A-D): Immunolocalization of $A\beta_{42}$; presence of $A\beta_{42}$ plaques (white arrowhead) (A-B) in the OB for $Ts_{(CO)}$. Objective magnification: 60x (A-B). (C): Immunoreactive $A\beta_{42\ in}$ the $Ts_{(VD3)}$ group, primarily in the EPL and GL. (D): Discrete immunoreactivity of Aβ42 in the $WT_{(CO)}$ group. Objective magnification: 40x Immunoblotting for (E,F): $A\beta_{42}$ and (E,G): caspase-3 p12.

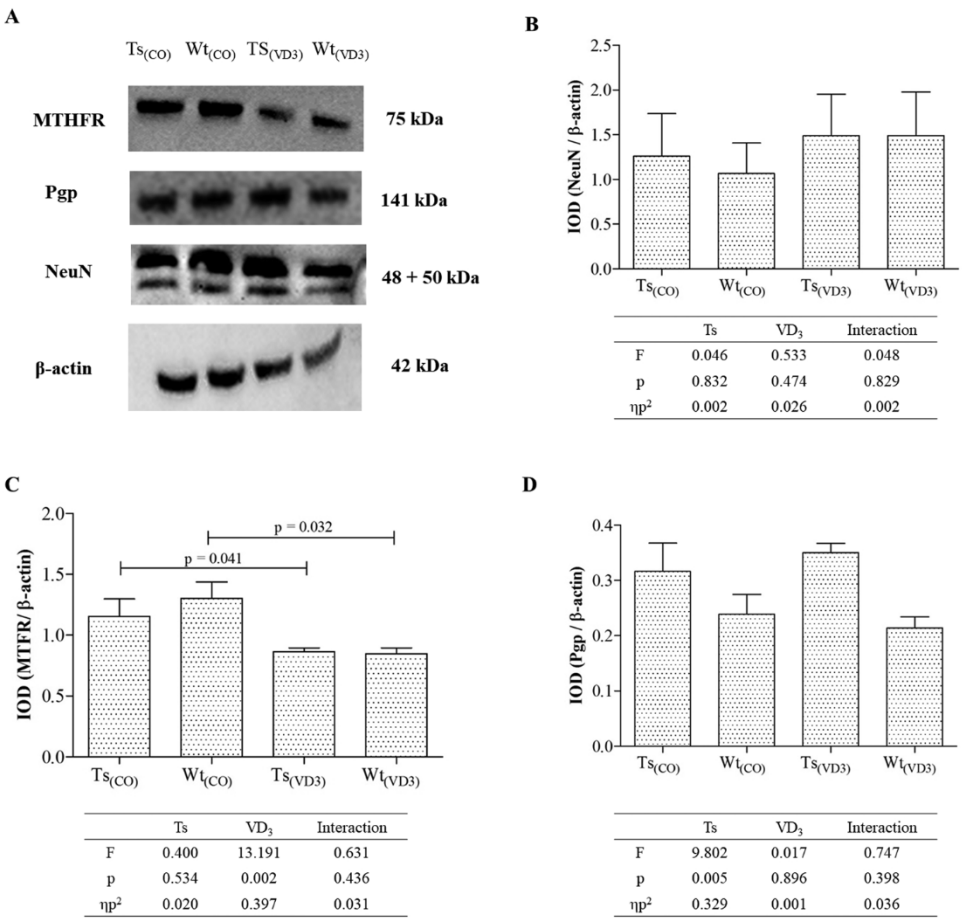

Fig. 4. (A): Immunoblotting for MTHFR, Pgp, and NeuN. Expression analysis of (B): NeuN, (C): MTHFR, and (D) Pgp.

$Ts_{(CO)}$ group, Fig. 5 presents the pattern of expression of APP in the C57BL/6 J mouse (Fig. 5A-E). The figure has been sourced from Allen Institute for Brain Sciences (2015), Allen Brain Atlas: Mouse Brain (https://mouse.brain-map.org/) and was adapted with permission from the Allen Brain Institute (http://www. alleninstitute. org/). It presents a comparison of APP in the C57BL/6 J mouse to the intrinsic increase in APP in the B6EiC3Sn-Rb(12. Ts171665Dn)2Cje/CjeDnJ models (Fig. 5F). Note that the deposition of Aβ42 in the EPL and mitral cells (black arrow) can lead to morphological and molecular changes (Fig. 5G-H). In Figs. 5I, 5J, and 5 K, the design reveals how the observed immunolocalization of Aβ42 may lead to possible functional effects in the olfactory bulb.

4. Discussion

During adulthood, individuals with DS exhibit severe impairments in olfactory function regarding odor discrimination, identification, and threshold (Cecchini et al., 2016). In the Ts65Dn mouse model, impairment of OB neurogenesis and olfactory function occurred in middle-aged mice (Bianchi et al., 2014). However, the mechanisms underlying these changes are not well understood. Considering that individuals with DS develop AD early in life (Head et al., 2012) and that olfactory dysfunction is one of the first clinical symptoms of AD (Zou et al., 2016; Roberts et al., 2016; Silva et al., 2018), knowledge regarding the effects of Aβ42 peptides on the morphological structure and other cellular mechanisms in the OB is crucial.

Under normal physiological conditions APP is expressed in different layers of the OB in C57BL/6 J mice (Allen Mouse Brain Atlas: https://mouse.brain-map.org/) (Fig. 5). This is presented in comparison to the Rb(12. Ts171665Dn)2Cje/CjeDnJ mice. Increased expression of APP (Villar et al., 2005) and its derivatives results in the increased production and accumulation of Aβ.

Thus, according to some reviews detailing the processing of olfactory information in the OB (Carleton et al., 2002; Nagayama et al., 2014), it is possible that the increase in Aβ42 can alter the morphology and expression of certain molecular markers in the OB, thus leading to olfactory dysfunction.

Therefore, given the role of glomeruli in the initial processing and transmission of information, it is possible that failure at this stage in response to an increase in Aβ42 could impair communication between OB cells, thus resulting in functional implications.

Morphologically, an intrinsic reduction in the EPL volume and number of mitral and granule cells was observed in trisomic mice. The EPL is largely neurophilic and plays an important role in processing olfactory information (Hamilton et al., 2005). This layer is composed of various cell types, including tuft cells and intrinsic interneurons (Hamilton et al., 2005; Nagayama et al., 2014). Olfactory signals are processed in the glomerulus and then transmitted to tuft cells and dendrites of mitral cells that extend into the EPL where further events occur to allow information to be processed in the OB (Nagayama et al., 2014).

Recently, a study demonstrated that the OB of Ts65Dn mice exhibits impaired neurogenesis (Bianchi et al., 2014). It is possible that this impairment affects the morphological structure of the tissue at the cellular level, thus affecting the morphology and number of some cell types and, at the same time, the volume of the OB layers, as observed in this study.

Nevertheless, positive effects on the MCL were observed after VD3 supplementation. VD3 contributes to an increase in the volume of the MCL and the number of granule cells. The MCL is composed of mitral cells that receive olfactory stimuli and participate in the regulation of

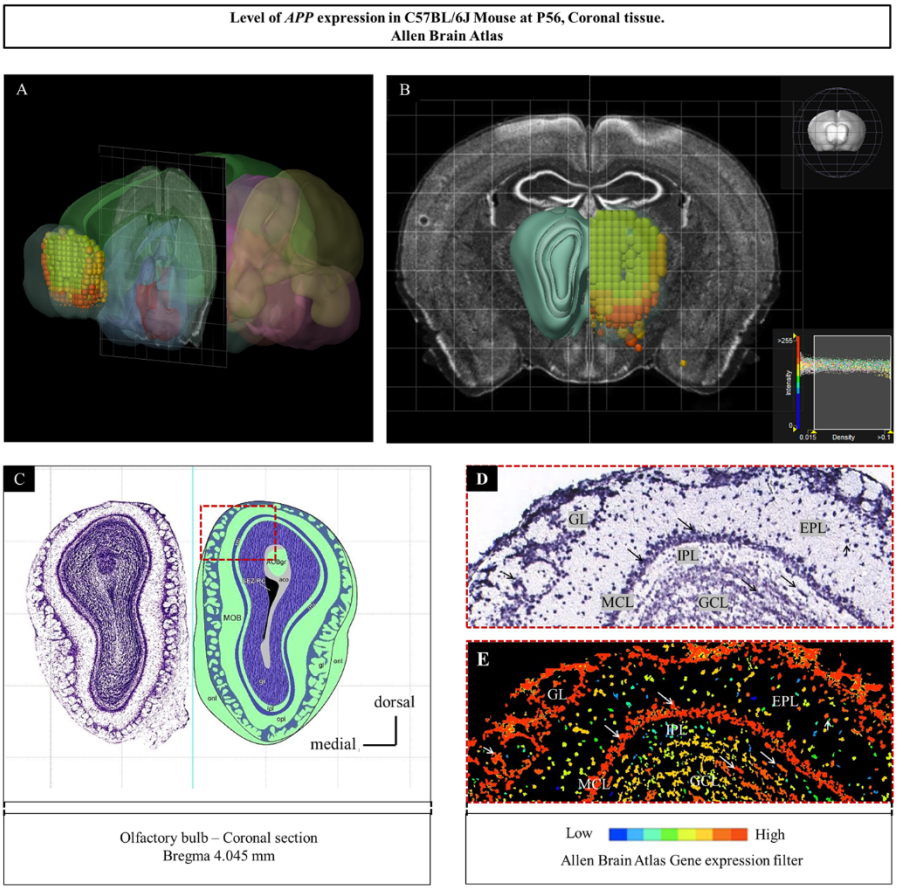

Fig. 5. *APP* expression levels in the different layers of the olfactory bulb (OB) of the C57BL/6 J mouse (Allen Mouse Brain Atlas: https://mouse.brain-map.org/) in comparison to levels in the model B6EiC3Sn-Rb(12. Ts171665Dn)2Cje/CjeDnJ. (A,B): Three-dimensional (3D) image of the brain presenting patterns of APP gene expression in OB layers (coronal: rostral to caudal). (C): Position 53 Coronal Plate (Bregma 4.045 mm) of the coronal sections of the OB stained with Nissl and delimitations of the olfactory layers. *In situ* hybridization image presenting (D): the cellular location of *APP* expression (black arrows) and (E): the level of expression detected in different layers of the OB (white arrows). (F): *APP* expression in a Ts65Dn model and in the human chromosome 21 (HSA 21). (G): Aβ42 immunolocalization and deposition (black arrows) in the OB layers in the $Ts_{(CO)}$ group. (H): Repercussions on the morphology possibly due to the increase in Aβ42 levels. (I,J): Schematic of synaptic connections in the mouse OB. (K): Implications that were possible in olfactory bulb in the $Ts_{(CO)}$ group. Glomerular layer (GL), external plexiform layer (EPL), mitral cell layer (MCL), internal plexiform layer (IPL), and granular cell layer (GCL). Glomeruli (G); periglomerular cells (PG); tufted cells (T); mitral cells (M). excitatory synapses (black arrow); PG cells (PG); Granules (G); inhibitory stimuli (purple arrow).

information directed to the olfactory cortex via axonal projections from the OB (Nagayama et al., 2014). Mitral cells represent a small percentage of cells in the MCL, and other cell types, including local interneurons such as granule cells, are observed in this layer (Panhuber et al., 1985; Nagayama et al., 2014).

Granular cells are abundant inhibitory interneurons in the OB and play an important role in processing olfactory information, including the inhibition of tuft and mitral cells via dendrodendritic synapses (Nunes and Kuner, 2015). Additionally, most newly formed cells in the OB become granule cells, and a small percentage of cells become periglomerular cells or astrocytes (Pignatelli and Belluzzi, 2010; Li et al., 2015; Lledo and Valley, 2016). Thus, considering that VD3 regulates a variety of neurotrophic factors that influence the process of differentiation, survival, growth, neuronal proliferation, and neurogenesis (Groves and Burne, 2017), VD3 supplementation exerted a positive effect on the number of granule cells and volume of the MCL as observed in treated mice.

In parallel with the morphological changes, we observed positive Aβ42 staining in the cytoplasm and intercellular space of all OB layers in the $Ts_{(CO)}$ group. The increased Aβ42 expression and Aβ42 staining with or without plaque formation in the different OB layers suggest a possible relationship between the morphological and molecular changes observed in the trisomic mice. Amyloid plaque accumulation and deposition have been demonstrated by immunohistochemistry in the OB and other brain regions of individuals with AD and in the Tg2576 AD mouse model (Zhang et al., 2010, Kenney et al., 2018). In APP/PS1 transgenic mouse models of AD, plaque deposition of Aβ42 impairs olfactory function and behavior (Yao et al., 2016). Therefore, based on the results of this study, it is likely that morphofunctional changes may occur in the OB of $Ts_{(CO)}$ in response to an increase in Aβ42.

Although VD3 supplementation did not significantly reduce Aβ42 expression in the OB of the $Ts_{(VD3)}$ group, it is important to highlight that deposits in the OB were not observed after VD3 supplementation. This indicate that a longer treatment period may, perhaps, significantly reduce Aβ42 expression in trisomic mice. The B6EiC3Sn-Rb(12, Ts171665Dn)2Cje model used in this study was genetically identical to the Ts65Dn model, and both possessed increased *APP* expression (Villar et al., 2005). Under normal physiological conditions, *APP* is expressed in the brains of humans and mice (Puig, Combs., 2013). Although the function of APP and its products are not clear, they play important roles in synaptic function and plasticity in the mouse brain (Nalivaeva and Turner, 2013). However, alterations in the processing and cleavage of APP induce the amyloidogenic pathway, ultimately leading to an increase in long Aβ fragments and resulting in the development of neuropathologies such as AD (Ludewig and Korte, 2017). Therefore, amyloid plates in the olfactory bulb may contribute to olfactory bulb dysfunction.

During neuropathological development, several markers, including caspase-3 p12, and signaling pathways are altered (Shen et al., 2017). Caspase-3 p12 was increased in the OB of $Ts_{(CO)}$ mice. However, VD3 supplementation reduced caspase-3 p12 expression in the $Ts_{(VD3)}$ and $Wt_{(VD3)}$ groups. In the brain, caspase-3 p12 is involved in the activation of apoptotic and pro-inflammatory signaling pathways (Kavanagh et al., 2014).

Additionally, caspase-3 plays an important role in APP degradation (Rohn and Head., 2009). The increase in caspase-3 indicates greater proteolytic processing of APP, production of Aβ peptides, loss of synapses, death of neurons, and development of AD (Gervais et al., 1999; Rohn and Head., 2009). In contrast, vitamin D reduces the activation of apoptotic mechanisms and markers, including caspase-3 (Yuan et al., 2018). In this context, the reduction in caspase-3 p12 in the treated groups suggests a beneficial effect of VD3 on the OB.

Other effects of VD3 supplementation included reduction of MTHFR expression. Thus, MTHFR can be considered an effector of VD3. MTHFR is involved in DNA synthesis, methylation, and repair mechanisms (Leclerc, 2013). Additionally, the MTHFR catalyzes the conversion of 5, 10-methylenetetrahydrofolate to 5-methyltetrahydrofolate. This co-substrate remediates homocysteine to methionine (Blom and Smulders., 2011). MTHFR deficiency has been associated with oxidative stress, neurotoxic accumulation of homocysteine, and reduced methylation capacity (Moretti and Caruso, 2019).

Other studies have demonstrated that *MTHFR* polymorphism leads to irregular homocysteine metabolism, contributes to hyperhomocysteinemia, and increases the risk for AD (Rai, 2017; Román et al., 2019). Increased homocysteine levels lead to a decrease in S-adenosyl-L-methionine levels (SAM), ultimately resulting in demethylation of DNA and overexpression of genes involved in the cleavage of APP, leading to an increase and deposition of Aβ42 (Román et al., 2019). Considering these results, the reduction in MTHFR levels in the brain after treatment may suggest that VD3 affects the expression of this protein in the brains of the $Ts_{(VD3)}$ and $Wt_{(VD3)}$ groups; however, further studies are required to investigate the effects of this reduction on the morphophysiology of the olfactory bulb.

Although some studies have demonstrated an increase in Pgp after VD3 treatment (Chow et al., 2011; Durk et al., 2014), we did not observe similar results between the experimental groups in this study. However, we did determine that the trisomy factor contributes to the increased expression of Pgp in OB. In the brains of mouse models of DS, the expression of enzymes involved in the clearance of Aβ, such as insulin-degrading enzyme and neprilysin, is not altered in the hippocampus (Wiseman et al., 2018); however, Pgp expression was not analyzed in the olfactory bulb in DS mouse models. Pgp is a protein that is expressed in the brain, primarily in the vasculature and astrocytes (Aryal et al., 2017). This protein and other transporters of the ATP-binding cassette (ABC) family are important elements of the blood-brain barrier (BBB) that prevents or minimizes the effects of toxic substances or components such as Aβ42 (Durk et al., 2014), which can enter or accumulate within the brain (Löscher and Potschka, 2005). In this study, the increased expression of Pgp in the OB of the $Ts_{(CO)}$ group may indicate that Pgp-mediated efflux must be increased to optimize Aβ42 clearance.

In our previous study (Gomes et al., 2019), we observed increased Pgp concentrations in the kidney tissue of trisomic mice treated with high doses of VD3. This finding suggests two important events: VD3 may act primarily by stimulating peripheral clearance of Aβ42 and the increase in peripheral clearance of Aβ42 in the kidney may help optimize the efflux of this peptide from peripheral tissues.

VD3 supplementation in the OB did not alter the NeuN protein expression in the experimental groups. NeuN is considered a marker of mature neurons (Gusel'nikova and Korzhevskiy, 2015). Mature neurons possess a specific mechanism to block apoptosis and ensure long-term survival (Kole et al., 2013). Moreover, the NeuN protein is expressed neither in the tuft or mitral cells (Weiler and Benali, 2005), nor during neuronal developmental stages (Francis et al., 1999). Thus, although morphological abnormalities were observed in trisomy mice, it is important to emphasize that these changes may also occur in other cell types that do not express NeuN.

Although high doses of VD3 have been demonstrated to affect morphology and certain target proteins in the olfactory bulb, it is important to consider possible side effects. Hence, our study is limited as the analysis of side effects such as monitoring of calcium and phosphate levels could allow for a better understanding of the systemic effects of high doses of VD3. However, in our previous study we observed a loss of body weight in VD3-treated groups (Gomes et al., 2019), thus suggesting the impact of high doses of VD3 in several metabolic pathways, including those investigated in this study.

5. Conclusion

Our results indicate the presence of certain morphological and molecular abnormalities in the OB of Ts mice, thus suggesting that Aβ42 plays a crucial role in morphofunctional abnormalities and may

potentially lead to functional impairment of the OB. However, treatment with high-dose VD3 attenuated some morphofunctional and molecular changes in the OB of Ts mice. Further studies are needed to evaluate the effects of high-dose VD3 in relation to other biomarkers and on the functional aspects of the olfactory bulb.

CRediT authorship contribution statement

Fabiana de Campos Gomes: Visualization, Conceptualization, Data curation, Formal analysis, Investigation, Methodology, Validation, Writing - original draft, Writing - review & editing. **Isabella Boechat Faria Santos:** Methodology, Writing – original draft, Writing – review & editing. **Carolinne Makino Stephani:** Methodology, Writing - original draft, Writing - review & editing. **Merari de Fátima Ramires Ferrari:** Methodology, Writing – original draft, Writing – review & editing, Resources. **Orfa Yineth Galvis-Alonso:** Methodology, Writing – original draft, Writing – review & editing. **Eny Maria Goloni-Bertollo:** Methodology, Writing – original draft, Writing – review & editing. **João Simão de Melo-Neto:** Conceptualization, Data curation, Formal analysis, Investigation, Methodology, Software, Writing - original draft, Writing - review & editing. **Érika Cristina Pavarino:** Methodology, Writing – original draft, Writing – review & editing, Project administration, Funding acquisition, Supervision.

Data Availability

Data will be made available on request.

Acknowledgments

This study was supported in part by the Coordenação de Aperfeiçoamento de Pessoal de Nível Superior - Capes - Finance Code 001 and the Conselho Nacional de Desenvolvimento Científico e Tecnológico (CNPq) grant number: 310806/2018-6. The authors thank the Laboratory of Experimental Immunology and Transplantation (Litex) and the Laboratory of Experimental Physiology, São José do Rio Preto Medical School (FAMERP) for their technical support.

Conflict of interest

The authors declare no conflicts of interest.

Appendix A. Supporting information

Supplementary data associated with this article can be found in the online version at doi:10.1016/j.tice.2022.101898.

References

Allen Institute for Brain Sciences 2015. Allen Brain Atlas: Brain Explorer 2 Available at: ⟨http://mouse.brain-map.org⟩. Accessed 15 April 2019.

Anjum, I., Jaffery, S.S., 2018. The Role of Vitamin D in Brain Health: A Mini Literature Review. Cureus 10 (7), e2960. https://doi.org/10.7759/cureus.2960.

Antonarakis, S.E., Lyle, R., Dermitzakis, E.T., Reymond, A., Deutsch, S., 2004. Chromosome 21 and down syndrome: from genomics to pathophysiology. Nat. Rev. Genet 5 (10), 725–738. https://doi.org/10.1038/nrg1448.

Aryal, M., Fischer, K., Gentile, C., Gitto, S., Zhang, Y.Z., McDannold, N., 2017. Effects on P-glycoprotein expression after blood-brain barrier disruption using focused ultrasound and microbubbles. Published 2017 Jan 3 PLoS One 12 (1), e0166061. https://doi.org/10.1371/journal.pone.0166061.

Bianchi, P., Bettini, S., Guidi, S., et al., 2014. Age-related impairment of olfactory bulb neurogenesis in the Ts65Dn mouse model of Down syndrome. Exp. Neurol. 251, 1–11. https://doi.org/10.1016/j.expneurol.2013.10.018.

Blom, H.J., Smulders, Y., 2011. Overview of homocysteine and folate metabolism. With special references to cardiovascular disease and neural tube defects. J. Inherit. Metab. Dis. 34 (1), 75–81. https://doi.org/10.1007/s10545-010-9177-4.

Carleton, A., Rochefort, C., Morante-Oria, J., et al., 2002. Making scents of olfactory neurogenesis. J. Physiol. Paris 96 (1–2), 115–122. https://doi.org/10.1016/s0928-4257(01)00087-0.

Cecchini, M.P., Viviani, D., Sandri, M., Hähner, A., Hummel, T., Zancanaro, C., 2016. Olfaction in people with down syndrome: a comprehensive assessment across four decades of age. PLoS One 11 (1), e0146486. https://doi.org/10.1371/journal.pone.0146486. Published 2016 Jan 5.

Chaves, J.C.S., Machado, F.T., Almeida, M.F., Bacovsky, T.B., Ferrari, M.F.R., 2020. microRNAs expression correlates with levels of APP, DYRK1A, hyperphosphorylated Tau and BDNF in the hippocampus of a mouse model for Down syndrome during ageing. Neurosci. Lett. 714, 134541.

Chen, M.A., Lander, T.R., Murphy, C., 2006. Nasal health in Down syndrome: a cross-sectional study. Otolaryngol. Head. Neck Surg. 134 (5), 741–745. https://doi.org/10.1016/j.otohns.2005.12.035.

Chhillar, N., Singh, N.K., Banerjee, B.D., Bala, K., Basu, M., Sharma, D., 2014. Intergenotypic variation of Vitamin B12 and Folate in AD: in north indian population. Ann. Indian Acad. Neurol. 17 (3), 308–312. https://doi.org/10.4103/0972-2327.138510.

Chow, E.C., Durk, M.R., Cummins, C.L., Pang, K.S., 2011. 1Alpha,25-dihydroxyvitamin D3 up-regulates P-glycoprotein via the vitamin D receptor and not farnesoid X receptor in both fxr(-/-) and fxr(+/+) mice and increased renal and brain efflux of digoxin in mice in vivo. J. Pharm. Exp. Ther. 337 (3), 846–859. https://doi.org/10.1124/jpet.111.179101.

Durk, M.R., Chan, G.N., Campos, C.R., et al., 2012. 1α,25-Dihydroxyvitamin D3-liganded vitamin D receptor increases expression and transport activity of P-glycoprotein in isolated rat brain capillaries and human and rat brain microvessel endothelial cells. J. Neurochem 123 (6), 944–953. https://doi.org/10.1111/jnc.12041.

Durk, M.R., Han, K., Chow, E.C., et al., 2014. 1α,25-Dihydroxyvitamin D3 reduces cerebral amyloid-β accumulation and improves cognition in mouse models of Alzheimer's disease. J. Neurosci. 34 (21), 7091–7101. https://doi.org/10.1523/JNEUROSCI.2711-13.2014.

Francis, F., Koulakoff, A., Boucher, D., et al., 1999. Doublecortin is a developmentally regulated, microtubule-associated protein expressed in migrating and differentiating neurons. Neuron 23 (2), 247–256. https://doi.org/10.1016/s0896-6273(00)80777-1.

Gervais, F.G., Xu, D., Robertson, G.S., et al., 1999. Involvement of caspases in proteolytic cleavage of Alzheimer's amyloid-beta precursor protein and amyloidogenic A beta peptide formation. Cell 97 (3), 395–406. https://doi.org/10.1016/s0092-8674(00)80748-5.

Gomes, F.C., de Melo-Neto, J.S., Ferrari, M.F.R., Carlos, C.P., Goloni-Bertollo, E.M., Pavarino, É.C., 2019. Vitamin D_3 increases the Caspase-3 p12, MTHFR, and P-glycoprotein reducing amyloid-β_{42} in the kidney of a mouse model for Down syndrome. Life Sci. 231, 116537.

Groves, N.J., Burne, T.H.J., 2017. The impact of vitamin D deficiency on neurogenesis in the adult brain. Neural Regen. Res 12 (3), 393–394. https://doi.org/10.4103/1673-5374.202936.

Gusel'nikova, V.V., Korzhevskiy, D.E., 2015. NeuN as a neuronal nuclear antigen and neuron differentiation marker. Acta Nat. 7 (2), 42–47.

Hamilton, K.A., Heinbockel, T., Ennis, M., Szabó, G., Erdélyi, F., Hayar, A., 2005. Properties of external plexiform layer interneurons in mouse olfactory bulb slices. Neuroscience 133 (3), 819–829. https://doi.org/10.1016/j.neuroscience.2005.03.008.

Han, X.J., Hu, Y.Y., Yang, Z.J., et al., 2017. Amyloid β-42 induces neuronal apoptosis by targeting mitochondria. Mol. Med Rep. 16 (4), 4521–4528. https://doi.org/10.3892/mmr.2017.7203.

Hartley, D., Blumenthal, T., Carrillo, M., et al., 2015. Down syndrome and Alzheimer's disease: common pathways, common goals. Alzheimers Dement 11 (6), 700–709. https://doi.org/10.1016/j.jalz.2014.10.007.

Head, E., Powell, D., Gold, B.T., Schmitt, F.A., 2012. Alzheimer's disease in Down Syndrome. Eur. J. Neurodegener. Dis. 1 (3), 353–364.

Head, E., Lott, I.T., Wilcock, D.M., Lemere, C.A., 2016. Aging in down syndrome and the development of Alzheimer's disease neuropathology. Curr. Alzheimer Res 13 (1), 18–29. https://doi.org/10.2174/1567205012666151020114607.

Hof, P.R., Bouras, C., Perl, D.P., Sparks, D.L., Mehta, N., Morrison, J.H., 1995. Age-related distribution of neuropathologic changes in the cerebral cortex of patients with Down's syndrome. Quantitative regional analysis and comparison with Alzheimer's disease. Arch. Neurol. 52 (4), 379–391. https://doi.org/10.1001/archneur.1995.00540280065020.

Hong, S., Quintero-Monzon, O., Ostaszewski, B.L., Podlisny, D.R., Cavanaugh, W.T., Yang, T., Holtzman, D.M., Cirrito, J.R., Selkoe, D.J., 2011. Dynamic analysis of amyloid β-protein in behaving mice reveals opposing changes in ISF versus parenchymal Aβ during age-related plaque formation. J. Neurosci.: Off. J. Soc. Neurosci. 31 (44), 15861–15869. https://doi.org/10.1523/JNEUROSCI.3272-11.2011.

Kavanagh, E., Rodhe, J., Burguillos, M.A., Venero, J.L., Joseph, B., 2014. Regulation of caspase-3 processing by cIAP2 controls the switch between pro-inflammatory activation and cell death in microglia. Published 2014 Dec 11 Cell Death Dis. 5 (12), e1565. https://doi.org/10.1038/cddis.2014.514.

Kenney, K., Iacono, D., Edlow, B.L., et al., 2018. Dementia after moderate-severe traumatic brain injury: coexistence of multiple proteinopathies. J. Neuropathol. Exp. Neurol. 77 (1), 50–63. https://doi.org/10.1093/jnen/nlx101.

Kole, A.J., Annis, R.P., Deshmukh, M., 2013. Mature neurons: equipped for survival. Published 2013 Jun 27 Cell Death Dis. 4 (6), e689. https://doi.org/10.1038/cddis.2013.220.

Landel, V., Annweiler, C., Millet, P., Morello, M., Féron, F., 2016. Vitamin D, cognition and Alzheimer's Disease: the therapeutic benefit is in the D-tails. J. Alzheimers Dis. 53 (2), 419–444. https://doi.org/10.3233/JAD-150943.

Leclerc, D., Sibani, S., Rozen, R., 2013. Molecular Biology of Methylenetetrahydrofolate Reductase (MTHFR) and Overview of Mutations/Polymorphisms. Madame Curie Bioscience Database. Austin (TX), Landes Bioscience, 2000. ⟨https://www.ncbi.nlm.nih.gov/books/NBK6561/⟩.

Li, Y.H., Feng, L., Zhang, G.X., Ma, C.G., 2015. Intranasal delivery of stem cells as therapy for central nervous system disease. Exp. Mol. Pathol. 98 (2), 145–151. https://doi.org/10.1016/j.yexmp.2015.01.016.

Löscher, W., Potschka, H., 2005. Blood-brain barrier active efflux transporters: ATP-binding cassette gene family. NeuroRx 2 (1), 86–98. https://doi.org/10.1602/neurorx.2.1.86.

Lucock, M., Thota, R., Garg, M., et al., 2018. Vitamin D and folate: a reciprocal environmental association based on seasonality and genetic disposition. Am. J. Hum. Biol. 30 (5), e23166 https://doi.org/10.1002/ajhb.23166.

Ludewig, S., Korte, M., 2017. Novel insights into the physiological function of the APP (Gene) family and its proteolytic fragments in synaptic plasticity. Front Mol. Neurosci. 9, 161. https://doi.org/10.3389/fnmol.2016.00161. Published 2017 Jan 20.

Moretti, R., Caruso, P., 2019. The controversial role of homocysteine in neurology: from labs to clinical practice. Int J. Mol. Sci. 20 (1), 231. https://doi.org/10.3390/ijms20010231. Published 2019 Jan 8.

Murphy, C., Jinich, S., 1996. Olfactory dysfunction in Down's syndrome. Neurobiol. Aging 17 (4), 631–637. https://doi.org/10.1016/0197-4580(96)00008-5.

Nagayama, S., Homma, R., Imamura, F., 2014. Neuronal organization of olfactory bulb circuits. Front Neural Circuits 8, 98. https://doi.org/10.3389/fncir.2014.00098. Published 2014 Sep 3.

Nalivaeva, N.N., Turner, A.J., 2013. The amyloid precursor protein: a biochemical enigma in brain development, function and disease. FEBS Lett. 587 (13), 2046–2054. https://doi.org/10.1016/j.febslet.2013.05.010.

Nunes, D., Kuner, T., 2015. Disinhibition of olfactory bulb granule cells accelerates odour discrimination in mice. Nat. Commun. 6, 8950. https://doi.org/10.1038/ncomms9950. Published 2015 Nov 23.

Panhuber, H., Laing, D.G., Willcox, M.E., Eagleson, G.K., Pittman, E.A., 1985. The distribution of the size and number of mitral cells in the olfactory bulb of the rat. J. Anat. 140 (Pt 2), 297–308. Pt 2.

Pignatelli, A., Belluzzi, O., 2010. Neurogenesis in the adult olfactory bulb. In: Menini, A. (Ed.), The Neurobiology of Olfaction. Boca Raton (FL): CRC Press, Taylor & Francis. Chapter 11. Available from. ⟨https://www.ncbi.nlm.nih.gov/books/NBK55966/⟩.

Puig, K.L., Combs, C.K., 2013. Expression and function of APP and its metabolites outside the central nervous system. Exp. Gerontol. 48 (7), 608–611. https://doi.org/10.1016/j.exger.2012.07.009.

Rai, V., 2017. Methylenetetrahydrofolate reductase (MTHFR) C677T polymorphism and Alzheimer disease risk: a meta-analysis. Mol. Neurobiol. 54 (2), 1173–1186. https://doi.org/10.1007/s12035-016-9722-8.

Rohn, T.T., Head, E., 2009. Caspases as therapeutic targets in Alzheimer's disease: is it time to "cut" to the chase? Int J. Clin. Exp. Pathol. 2 (2), 108–118.

Roberts, R.O., Christianson, T.J., Kremers, W.K., et al., 2016. Association between olfactory dysfunction and amnestic mild cognitive impairment and Alzheimer Disease Dementia published correction appears in JAMA Neurol. 2016 Apr;73(4):481]. JAMA Neurol. 73 (1), 93–101.

Román, G.C., Mancera-Páez, O., Bernal, C., 2019. Epigenetic factors in late-onset Alzheimer's disease: *MTHFR* and *CTH* gene polymorphisms, metabolic transsulfuration and methylation pathways, and B vitamins. Int J. Mol. Sci. 20 (2), 319. https://doi.org/10.3390/ijms20020319. Published 2019 Jan 14.

Salbaum, J.M., Kappen, C., 2012. Genetic and epigenomic footprints of folate. Prog. Mol. Biol. Transl. Sci. 108, 129–158. https://doi.org/10.1016/B978-0-12-398397-8.00006-X.

Shen, X., Burguillos, M.A., Joseph, B., 2017. Guilt by association, caspase-3 regulates microglia polarization. Cell Cycle 16 (4), 306–307. https://doi.org/10.1080/15384101.2016.1254979.

Silva, M.M.E., Mercer, P.B.S., Witt, M.C.Z., Pessoa, R.R., 2018. Olfactory dysfunction in Alzheimer's disease Systematic review and meta-analysis. Dement Neuropsychol. 12 (2), 123–132. https://doi.org/10.1590/1980-57642018dn12-020004.

Schupf, N., Lee, J.H., Pang, D., et al., 2018. Epidemiology of estrogen and dementia in women with Down syndrome. Free Radic. Biol. Med 114, 62–68. https://doi.org/10.1016/j.freeradbiomed.2017.08.019.

Spellicy, C.J., Northrup, H., Fletcher, J.M., et al., 2012. Folate metabolism gene 5,10-methylenetetrahydrofolate reductase (MTHFR) is associated with ADHD in myelomeningocele patients. PLoS One 7 (12), e51330. https://doi.org/10.1371/journal.pone.0051330.

Ter Laak, H.J., Renkawek, K., van Workum, F.P., 1994. The olfactory bulb in Alzheimer disease: a morphologic study of neuron loss, tangles, and senile plaques in relation to olfaction. Alzheimer Dis. Assoc. Disord. 8 (1), 38–48.

Tsutiya, A., Watanabe, H., Nakano, Y., Nishihara, M., Goshima, Y., Ohtani-Kaneko, R., 2016. Deletion of collapsin response mediator protein 4 results in abnormal layer thickness and elongation of mitral cell apical dendrites in the neonatal olfactory bulb. J. Anat. 228 (5), 792–804. https://doi.org/10.1111/joa.12434.

Villar, A.J., Belichenko, P.V., Gillespie, A.M., Kozy, H.M., Mobley, W.C., Epstein, C.J., 2005. Identification and characterization of a new Down syndrome model, Ts[Rb (12.1716)]2Cje, resulting from a spontaneous Robertsonian fusion between T(171) 65Dn and mouse chromosome 12. Mamm. Genome 16 (2), 79–90. https://doi.org/10.1007/s00335-004-2428-7.

Zhang, X.M., Xiong, K., Cai, Y., et al., 2010. Functional deprivation promotes amyloid plaque pathogenesis in Tg2576 mouse olfactory bulb and piriform cortex. Eur. J. Neurosci. 31 (4), 710–721. https://doi.org/10.1111/j.1460-9568.2010.07103.x.

Zhang, J.W., Pang, B., Zhao, Q., et al., 2018. Hyperhomocysteinemia induces injury in olfactory bulb neurons by downregulating Hes1 and Hes5 expression. Neural. Regen. Res. 13 (2), 272–279. https://doi.org/10.4103/1673-5374.220779.

Zou, Y.M., Lu, D., Liu, L.P., Zhang, H.H., Zhou, Y.Y., 2016. Olfactory dysfunction in Alzheimer's disease. Neuropsychiatr. Dis. Treat. 12, 869–875. https://doi.org/10.2147/NDT.S104886. Published 2016 Apr 15.

Zhuang, X., Silverman, A.-J., Silver, R., 1999. Distribution and local differentiation of mast cells in the parenchyma of the forebrain. J. Comp. Neurol. 408, 477–488. https://doi.org/10.1002/(SICI)1096-9861(19990614)408:4<477::AID-CNE3>3.0.CO;2-O.

Weiler, E., Benali, A., 2005. Olfactory epithelia differentially express neuronal markers. J. Neurocytol. 34 (3–5), 217–240. https://doi.org/10.1007/s11068-005-8355-z.

Wiseman, F.K., Pulford, L.J., Barkus, C., et al., 2018. Trisomy of human chromosome 21 enhances amyloid-β deposition independently of an extra copy of APP [published correction appears in Brain. Brain 141 (8), 2457–2474. https://doi.org/10.1093/brain/awy159.

Weibel, E.R., Kistler, G.S., Scherle, W.F., 1966. Practical stereological methods for morphometric cytology. J. Cell Biol. 30 (1), 23–38. https://doi.org/10.1083/jcb.30.1.23.

Wergeland, S., Torkildsen, Ø., Myhr, K.M., Aksnes, L., Mørk, S.J., Bø, L., 2011. Dietary vitamin D3 supplements reduce demyelination in the cuprizone model. PLoS One 6 (10), e26262. https://doi.org/10.1371/journal.pone.0026262.

Yao, Z.G., Jing, H.Y., Wang, D.M., et al., 2016. Valproic acid ameliorates olfactory dysfunction in APP/PS1 transgenic mice of Alzheimer's disease: ameliorations from the olfactory epithelium to the olfactory bulb. Pharm. Biochem Behav. 144, 53–59. https://doi.org/10.1016/j.pbb.2016.02.012.

Yuan, J., Guo, X., Liu, Z., et al., 2018. Vitamin D receptor activation influences the ERK pathway and protects against neurological deficits and neuronal death. Int. J. Mol. Med. 41 (1), 364–372. https://doi.org/10.3892/ijmm.2017.3249.